Indian Journal of Chemistry
Vol. 55A, September 2016, pp. 1084-1089

Sodium polystyrene sulfonate template assisted hydrothermal synthesis of hydroxyapatite nanorods

Pakvipar Chaopanich[a] & Punnama Siriphannon [a, b, *]

[a]Department of Chemistry, Faculty of Science, King Mongkut's Institute of Technology Ladkrabang, Chalongkrung Road, Ladkrabang, Bangkok 10520, Thailand

[b]Functional Nanostructured Materials Laboratory, College of KMITL Nanotechnology, King Mongkut's Institute of Technology Ladkrabang, Chalongkrung Road, Ladkrabang, Bangkok 10520, Thailand

Email: punnama.si@kmitl.ac.th

Received 8 February 2016; revised and accepted 31 August 2016

Hydroxyapatite nanoparticles (nHAp) have been synthesized by benign hydrothermal reaction from the aqueous mixture of $Ca(NO_3)_2{\cdot}4H_2O$ and $(NH_4)_2HPO_4$ solutions in the presence of non-toxic sodium polystyrene sulfonate (PSS) template. The *p*H of starting precursors has been adjusted to 10.5 before hydrothermal treatment at 100°C for 1, 2 and 3 h. The added PSS template generates the largely negative surface of dicalcium phosphate dihydrate (DCPD) precursor, resulting in minimization of precursor agglomeration and promoting the hydrothermal growth of nHAp along preferential *c*-axis as rod-shaped crystals. The crystallite sizes along 002-plane of nHAp synthesized with and without PSS template are 47.1 and 29.5 nm, respectively. With longer hydrothermal treatment time, larger crystallite size of nHAp is obtained. *In vitro* cytotoxicity of the synthesized nHAp has been evaluated by MTT assay using African green monkey kidney fibroblast cells, in which the nHAp exhibits low cytotoxicity. Antibacterial activities of the synthesized nHAp against *S.aureus* and *E.coli* have been tested. Due to the presence of largely negative surface, the nHAp could inhibit only the gram-positive *S.aureus*, creating a clear zone of about 9.5 mm.

Keywords: Hydroxyapatite nanoparticles, Hydrothermal synthesis, Polyelectrolytes, Nanorods

Hydroxyapatite (HAp, $Ca_{10}(PO_4)_6(OH)_2$) is one of the most important calcium phosphate based inorganic biomaterials due to its similarity to human hard tissues. However, the main disadvantages of HAp are low fracture toughness and flexural strength[1,2]; therefore, it has been commonly used in powder, coating and non-load bearing applications. In addition, HAp having plate-like or rod-like crystals with grain size less than 100 nm has been reported mimicking the structure of physiological hard tissues[3,4]. Thus, the nanosized HAp is considered to be the best material for long term using in medical applications[5-6]. The nanosized HAp also showed much higher bioactivity than the microsized HAp[7-9].

In view of the merits of nanosized HAp mentioned above, many researchers have studied and developed various methods for synthesis nanosized HAp[10-13]. Amongst these, the template addition is one of the most attractive method because the templates could facilitate the formation of nanosized particles with diminished degree of agglomeration and controlled their morphologies. Various kinds of templates have been reported, e.g. natural biomacromolecules[14], polymers[15-17], surfactants[13,18], etc.

Among various polymer templates, polyelectrolytes have attracted much attention as tools for tailoring nanostructures especially in biomedical applications[19,20]. Therefore, sodium polystyrene sulfonate (PSS), which is a linear polyelectrolyte, has been used as template for synthesis of nanosized HAp in the present study. Since the PSS is a water-soluble strong anionic polyelectrolyte carrying negative charges on its backbone, the presence of PSS molecules in the synthesis system was considered to play an important role in nucleation and growth of HAp crystals. The PSS template was also used in our previous research for the synthesis of nano HAp by refluxing method[13]. The presence of PSS in the refluxing system could control the HAp growth along the 002-plane, resulting in the reduction of HAp crystallite size[13], and hence the PSS template was applied to the hydrothermal synthesis of HAp in order to investigate its effect on HAp growth in the closed system of internally pressurized autoclave, this synthesis method being a facile and environmentally benign process. The hydrothermal reaction time was varied in order to investigate its effect on HAp crystallite size and morphology. In addition, ***in vitro*** cytotoxicity and antibacterial activities of the synthesized HAp were also tested.

Experimental

$(NH_4)_2HPO_4$ (99%, Fisher Scientific) and $Ca(NO_3)_2{\cdot}4H_2O$ (99%, Ajax Finechem) were used as starting materials for synthesis of hydroxyapatite (HAp). An anionic polyelectrolyte, i.e., sodium

polystyrene sulfonate (PSS, 18 wt% aqueous solution, Sigma Aldrich), was used as templating agent in the HAp synthesis. NaOH (97%) used for adjusting of *p*H and ethanol (99.9%) as washing solvent were purchased from Carlo Erba.

The hydroxyapatite nanoparticles (nHAp) were synthesized by template-assisted hydrothermal method. Firstly, 10 mL of 0.2 % *w/v* PSS solution was pre-mixed with 25 mL of 0.2 mol/L $Ca(NO_3)_2{\cdot}4H_2O$ aqueous solution at room temperature. Then, 25 mL of 0.12 mol/L $(NH_4)_2HPO_4$ aqueous solution was added dropwise into the pre-mixed solution with continuous stirring for 30 min at room temperature. The starting mixtures were controlled at concentrations corresponding to the molar stoichiometric HAp, i.e., Ca/P molar ratio = 1.67. The *p*H of the starting mixtures was adjusted to 10.5 by adding 0.5 mol/L of NaOH solution, resulting in the formation of white suspensions. Subsequently, the white suspensions were transferred to Teflon-lined stainless steel autoclave of 50 mL capacity and subjected to hydrothermal treated in an oven at 100 °C for 1, 2 and 3 h. The hydrothermal precipitates were separated by centrifugation (2374 g for 5 min), washed with distilled water and ethanol for several times and then dried in an oven at 45 °C for 24 h. The nHAp sample obtained after 3 h hydrothermal treatment in the PSS-free system was designated as P0.0H3, while those obtained after 1, 2 and 3 h hydrothermal treatment in the PSS system were respectively designated as P0.2H1, P0.2H2 and P0.2H3.

X-ray diffractometer (XRD; D8 Advance, Bruker AG) was used for investigation the crystalline phase of the synthesized nHAp. The XRD characterization was performed using CuKα radiation (λ = 1.54 Å) at *2* range of 20^o–60^o with step size of 0.04°/step and scanning speed of 1°/s. Surface charge of the synthesized nHAp was determined by zeta potential analyzer (Delsa^{TW} Nano Beckman Coulter, Inc.). The zeta potential ( ) measurement was performed in triplicate using the dispersion of nHAp in phosphate buffered solution (PBS) at *p*H 7.4. Morphology and selected area electron diffraction (SEAD) of the synthesized nHAp were investigated by transmission electron microscope (TEM; JEM 2010, JEOL).

In vitro cytotoxicity of the synthesized nHAp against African green monkey kidney fibroblasts (Vero cells) was evaluated by MTT assay for primary screening. The testing was performed according to ISO 10993-5[21]. Antibacterial activity of the synthesized nHAp against ***Staphylococcus aureus*** ATCC®25923 ***(S. aureus)*** and ***Escherichia coli*** ATCC®25922 ***(E. coli)*** were tested by disc diffusion method using agar medium. The testing was performed according to the Performance Standards for Antimicrobial Susceptibility Testing, M100-21[22].

Results and discussion

Figure 1 and Table 1 show the XRD patterns and the zeta potential ( ) values of the starting precursors and the nHAp synthesized without and with PSS template by hydrothermal treatment at *p*H 10.5 for 3 h. It can be seen that the crystalline peaks of both starting precursors in the systems with and without PSS template correspond to dicalcium phosphate dihydrate ($CaHPO_4{\cdot}2H_2O$ or DCPD) in JCPDS No. 09-0077. The formation of DCPD precursor is shown below:

$$Ca^{2+} + HPO_4^{2-} + 2H_2O \rightarrow CaHPO_4{\cdot}2H_2O$$

Although the starting precursors for both systems were DCPD, their values were quite different, indicating difference in their surface charge. The value of Pre-P0.0H3 without PSS template was positive, but that of Pre-P0.2H3 with PSS template was largely negative. These results suggested that the presence of anionic PSS template generated the

Table 1 – Phase composition, zeta potential and crystallite size of the starting precursors and the nHAp synthesized without and with PSS template

System	Sample	Phase composition	Zeta potential (mV)	Crystallite size[a] $_{002}$ (nm)
	Pre-P0.0H3	DCPD [b]	+6.04	n/a
Without PSS template	P0.0H3	HAp	+2.01	29.5
	P0.0R3 [c]	HAp	-4.34	30.9
	Pre-P0.2H3	DCPD	-20.63	n/a
With PSS template	P0.2H3	HAp	-19.52	47.1
	P0.2R3 [c]	HAp	+5.46	28.3

[a]Calculated by Scherrer's equation.
[b]DCPD : dicalcium phosphate dihydrate ($CaHPO_4{\cdot}2H_2O$).
[c]Synthesized by refluxing method in the previous study[13].

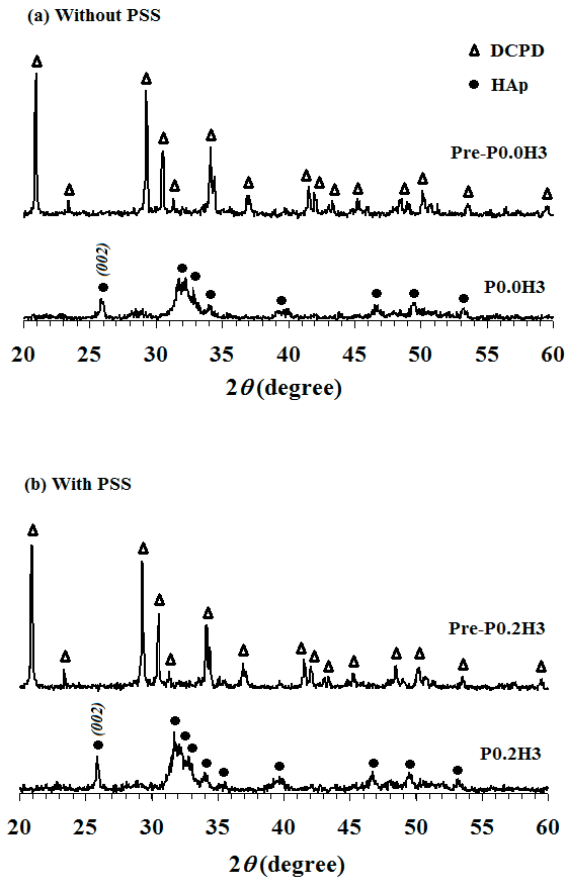

Fig. 1 – XRD patterns of the starting precursors and the nHAp synthesized at *p*H 10.5 for 3 h. [(a) without PSS template; (b) with PSS template].

negative charged particles. After hydrothermal treatment, the XRD patterns of P0.0H3 and P0.2H3 revealed that both Pre-P0.0H3 and Pre-P0.2H3 precursors transformed to monophasic hydroxyapatite, corresponding to JCPDS No. 74-565 (Fig. 1). The hydrothermal transformation of DCPD is as shown below:

$$10CaHPO_4{\cdot}2H_2O \rightarrow Ca_{10}(PO_4)_6(OH)_2 + 4PO_4^{3-} + 18H_2O + 12H^+$$

In addition, the XRD patterns of P0.0H3 and P0.2H3 exhibit broad crystalline peaks, representing the formation of hydroxyapatite nanocrystals. The crystallite sizes of the synthesized nHAp along 002-plane were calculated by Scherrer's equation and summarized in Table 1.

$$\tau = \frac{k\lambda}{\beta cos\theta} \quad ..(1)$$

where is crystallite size (Å), *k* is shape constant(~ 0.9),

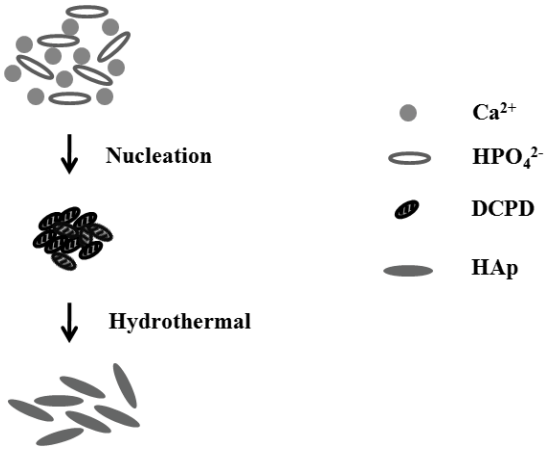

Fig. 2 – Schematic representation of hydrothermal synthesis of nHAp (without PSS template).

λ is the CuK wavelength (Å), is the Bragg's angle (degree) and β is the observed full width at half maximum of peak at 2 =25.8°. It can be seen that the crystallite size along 002-plane of P0.0H3 is smaller than that of P0.2H3, suggesting the effect of PSS template on the crystal growth along *c*-axis. In the PSS-free system, the Pre-P0.0H3 precursor has relatively low positive value that might lead to the agglomeration of precursor particles as shown in Fig. 2, resulting in the confinement of hydroxyapatite crystal growth during hydrothermal treatment.

On the other hand, the Pre-P0.2H3 precursor with the PSS template has largely negative value, in which this highly charged surface could prevent the agglomeration of precursor particles and the hydroxyapatite crystals could grow freely along their preferred direction, resulting in the larger crystallite size in the P0.2H3 sample.

Figure 3 shows the mechanism of nHAp formation in the presence of PSS template. The stretched chain conformation of PSS template was obtained in the aqueous solution due to the strong Coulombic repulsive force between the negative charged sulfonic groups ($-SO_3^-$) on the backbone of PSS chains. After adding the Ca^{2+} solution into the PSS solution, the Ca^{2+} ions spontaneously combined with the negatively charged $-SO_3^-$ groups of PSS template, forming the PSS-Ca intermediate. Then, on addition of the HPO_4^{2-} solution, the HPO_4^{2-} ions would interact with the PSS-Ca intermediate to create the DCPD precursor on the rigid-rod PSS chains. Finally, the DCPD precursor acted as the nucleation site for nHAp growth.

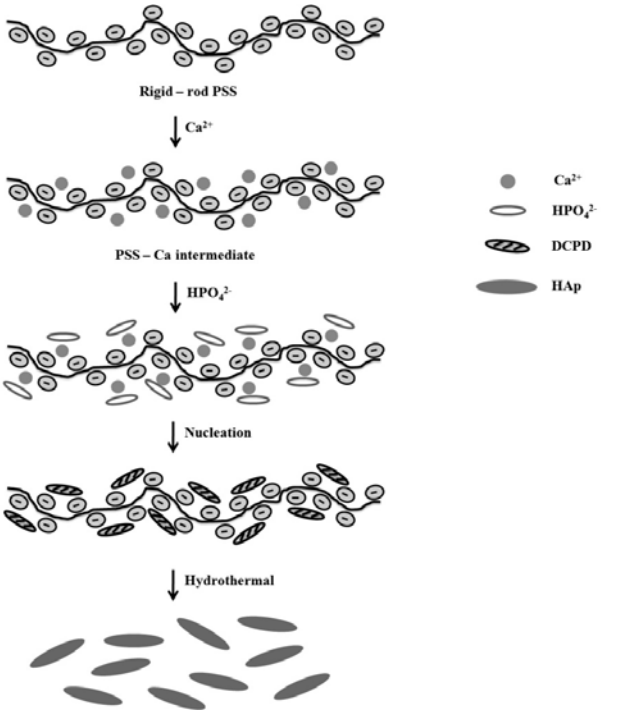

Fig. 3 – Schematic representation of hydrothermal synthesis of nHAp (with PSS template).

From the above mentioned crystallite sizes and values of nHAp obtained from the hydrothermal synthesis, it may be concluded that the presence of PSS template could promote the nHAp crystals growth along their preferred direction. However, the effect of PSS on the crystallite sizes and values of hydrothermally synthesized nHAp were different from those prepared by refluxing method as reported in our previous work[13] (Table 1). In the refluxing method, the presence of PSS template brought about only slight changes in the crystallite sizes and values. On the other hand, in the hydrothermal synthesis, the crystallite size of nHAp was significantly increased and the value of nHAp was drastically changed due to the presence of PSS template. These significant changes were considered to be due to the synergistic effects of the PSS template and the closed pressurized hydrothermal system. Since the PSS template could primarily interact with the Ca^{2+} ions to form the PSS-Ca intermediate as discussed above, it could bring about the reduction of free Ca^{2+} ions in the solution. The closed pressurized system concurrently affected the restricted movement of PSS-Ca intermediate during the hydrothermal reaction, which is different from the

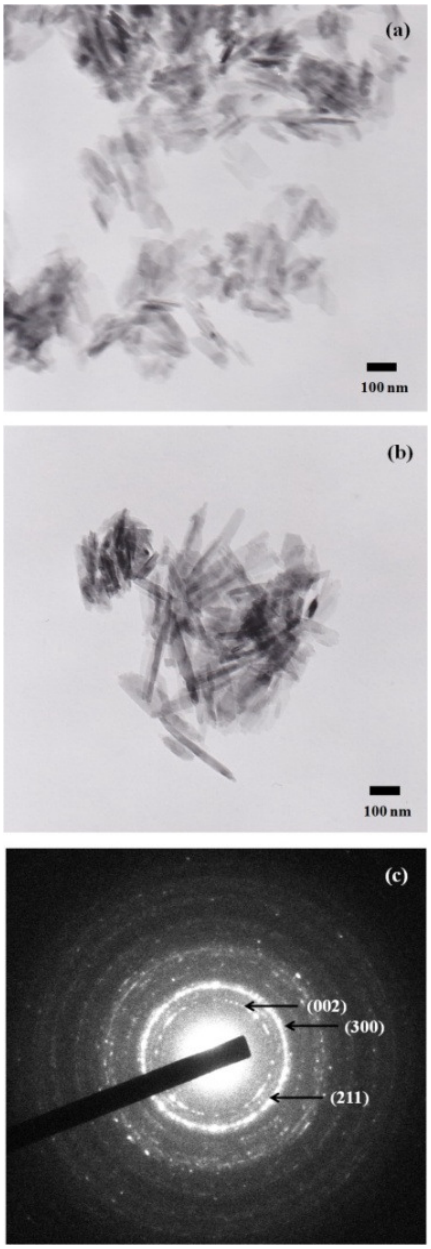

Fig. 4 - TEM images of the synthesized nHAp. [(a) P0.0H3; (b) P0.2H3; (c) SAED pattern of P0.2H3].

refluxing system. The constrained PSS-Ca intermediate in the hydrothermal system resulted in further formation of the constrained DCPD precursor. Therefore, the growth of nHAp was mainly from the integration of adjacent DCPD nucleation sites along the *c*-axis direction.

Figure 4(a) and 4(b) respectively show the TEM images of the P0.0H3 and P0.2H3 samples. The irregular rod-shaped hydroxyapatite crystals were observed in the P0.0H3 sample, while the longer rod-

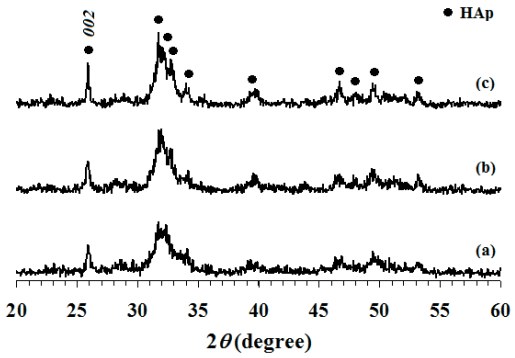

Fig. 5 – XRD patterns of the synthesized nHAp at various reaction times. [(a) P0.2H1; (b) P0.2H2; (c) P0.2H3].

shaped crystals were observed in the P0.2H3 sample. These results are in agreement with the calculated crystallite size along 002-plane as previously discussed. The selected area electron diffraction (SAED) of the P0.2H3 sample in Fig.4(c) shows the characteristic ring pattern of polycrystalline hydroxyapatite. The broad diffuse ring corresponding to the (112), (211) and (300) reflections were in agreement with the broad crystalline peaks at 2 ~31°–34° in the XRD pattern. In addition, an incomplete ring corresponding to (002) reflection was also observed, showing the preferential growth of hydroxyapatite along *c*-axis.

Figure 5 shows the XRD patterns of the nHAp synthesized by using 0.2% *w/v* PSS template at *p*H 10.5 and hydrothermal treatment for 1 h, 2 h and 3 h. It can be seen that diffraction peaks of synthesized nHAp in Fig. 5(a)-(c) correspond to the hydroxyapatite phase (JCPDS No.74-565). There are no peaks of DCPD precursor nor other impurities observed in the XRD patterns of the hydrothermal nHAp products. These results reveal that the DCPD phase in the P0.2H0 precursor transformed to crystalline hydroxyapatite phase even after hydrothermal treatment for only 1 h. The crystallite sizes along 002-plane of P0.2H1, P0.2H2 and P0.2H3 calculated from the Scherrer's equation were 23.6 nm, 28.0 nm and 47.1 nm, respectively. On longer hydrothermal treatment time, larger crystallite size of nHAp was obtained.

Figure 6 shows the morphologies of P0.2H1, P0.2H2 and P0.2H3 samples. In Fig. 6(a), the P0.2H1 sample was composed of the agglomerated clusters of rod-shaped hydroxyapatite nanocrystals. After prolonged hydrothermal treatment, the longer rod-

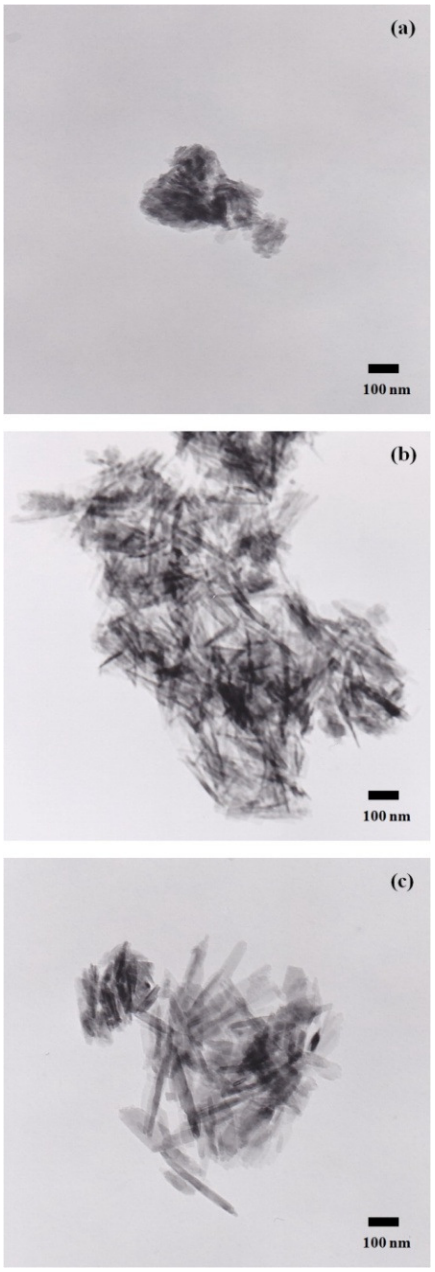

Fig. 6 – TEM images of the nHAp synthesized in the presence of 0.2 wt% PSS at various reaction times at *p*H 10.5. [(a) P0.2H1; (b) P0.2H2; (c) P0.2H3].

shaped hydroxyapatite nanocrystals were obtained as observed in Fig. 6(b) and 6(c), concomitant with the higher relative intensity of 002 peaks in Fig. 5(b) and 5(c). These results suggest that the prolonged hydrothermal treatment could promote the preferential growth of hydroxyapatite along *c*-axis.

The *in vitro* cytotoxicity of P0.2H3 sample against Vero cells was evaluated by MTT assay for primary screening using cell concentration of 1,000 g/mL. It

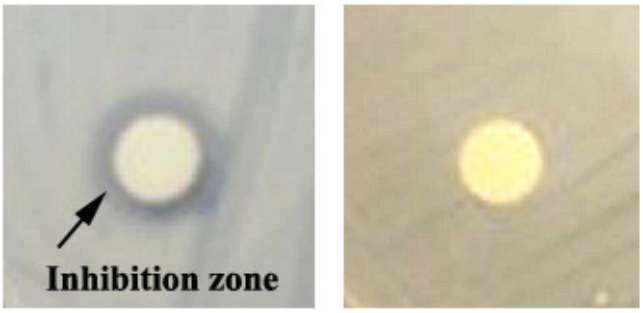

Fig. 7 – Antibacterial activity of the P0.2H3. [*S. aureus* (left); *E. coli* (right)].

was found that the percentage growth inhibition of P0.2H3 was 13.78%, indicating its low cytotoxicity against Vero cells[23]. In addition, some research works have reported that the HAp particles with negative zeta potential can promote the attachment and proliferation of bone cells[24], therefore, the P0.2H3 with -19.52 mV was considered to be biocompatible material.

The antibacterial activity of P0.2H3 sample was investigated by agar disc diffusion method using *Staphylococcus aureus* ATCC®25923 *(S. aureus)* and *Escherichia coli* ATCC®25922 *(E. coli)* as model organisms. Figure 7(a) shows the inhibition zone of about 9.5 mm around the P0.2H3 sample for *S. aureus*. On the other hand, there was no inhibition zone around the P0.2H3 sample for *E. coli* as shown in Fig. 7(b). These results are attributed to the effect of negative surface charge P0.2H3 sample, in which it could effectively interact with the gram-positive *S. aureus*, but not the gram- negative *E. coli*.

In the present study, the HAp nanorods were successfully synthesized by benign hydrothermal reaction with the assistance of the PSS template. The PSS template played an important role in nucleation and growth mechanisms of HAp, resulting in the formation of rod-like HAp nanocrystals as the PSS template could promote the preferential growth along *c*-axis. With longer hydrothermal reaction time, larger crystallite size of HAp nanorod was obtained. The HAp nanorods synthesized with the PSS template exhibited low *in vitro* cytotoxicity for the African green monkey kidney fibroblast cells and effectively inhibited the growth of gram-positive *S. aureus* bacteria.

Acknowledgement

The authors acknowledge the financial support from the Office of the Higher Education Commission, Ministry of Education, Thailand, under the research project title “Higher Education Research Promotion”.

References

1 Jarcho M, Bolen C H, Thomas M B, Bobick J, Kay J F & Doremus R H, *J Mater Sci*, 11 (1976) 2027.
2 Dewith G, Vandijk H J A, Hattu N & Prijs K, *J Mater Sci*, 16 (1981) 1592.
3 Cai Y, Liu Y, Yan W, Hu Q, Tao J, Zhang M, Shi Z & Tang R, *J Mater Chem*, 17 (2007) 3780.
4 Tiselius A, Hjerten S & Levin O, *Arch Biochem Biophys*, 65 (1995) 132.
5 Cheng K, Weng W, Han G, Du P, Shen G, Yang J & Ferreira J M F, *Mater Res Bull*, 38 (2003) 89.
6 Cheng K, Shen G, Weng W, Han G & Ferreira J M F, *Mater Lett*, 51 (2001) 37.
7 Perla V & Webster T J, *Int J Nanomedicine*, 1 (2006) 351.
8 Roy M, Bandyopadhyay A & Bose S, *Surf Coat Technol*, 205 (2011) 2785.
9 Stupp S I & Ciegler G W, *J Biomed Mater Res*, 26 (1992) 169.
10 Bose S & Saha S K, *J Am Ceram Soc*, 86 (2003) 1055.
11 Shih W J, Chen Y F, Wang M C & Hon M H, *J Cryst Growth*, 270 (2004) 211.
12 Lim G K, Wang J, Ng S C, Chew C H & Gan L M, *Biomaterials*, 18 (1997) 1433.
13 Chaopanich P & Siriphannon P, *Aust J Chem*, 68 (2015) 1293.
14 Tsetsekou A, Brasinika D, Vaou V & Chatzitheodoridis E, *Mater Sci Eng C*, 43 (2014) 555.
15 Ye F, Guo H, Zhang H & He X, *Acta Biomater*, 6 (2010) 2212.
16 Li J J, Chen Y P, Yin Y J, Yao F L & Yao K D, *Biomaterials*, 28 (2007) 781.
17 Zhang F, Zhou Z H, Yang S P, Mao L H, Chen H M & Yu X B, *Mater Lett*, 59 (2005) 1422.
18 Coelho J M, Moreira J A, Almeida A & Monteiro F J, *J Mater Sci: Mater Med*, 21 (2010) 2543.
19 Tang Z, Wang Y, Podsiadlo P & Kotov A, *Adv Mater*, 18 (2006) 3203.
20 Boudou T, Crouzier T, Ren K, Blin G & Picart C, *Adv Mater*, 26 (2010) 441.
21 ISO 10993-5:2009 Biological evaluation of medical devices Part 5: Tests for in vitro cytotoxicity by the International Organization for Standardization, pp. 24 – 28.
22 Performance Standards for Antimicrobial Susceptibility Testing: Twenty-First Informational Supplement M100–S21 2011, Clinical and Laboratory Standards Institute, (CLSI: Wayne, PA).
23 Gad S C, *Alternatives to in vivo Studies in Toxicology*, (Grove’s dictionari’s Inc., USA), p. 178.
24 Doostmohammadi A, Monshi A, Salehi R, Fathi M H, Karbasi S, Pieles U & Daniels A U, *Mater Chem Phys*, 132 (2012) 446.